PAPER

Check for updates

Hybrid nanomaterial inks for printed resistive temperature sensors with tunable properties to maximize sensitivity†

Muhammadeziz Tursunniyaz, [ID] [a] Vasvi Agarwal,[b] Anna Meredith[b] and
Joseph Andrews*[a,b]

Nanomaterial-based inks are one of the essential building blocks for printed electronics. Inks consisting of silver nanoparticles have been well received as conductive inks for printed electronics among researchers and industry due to their good electrical performance, relatively low sintering temperature, and wide range of commercial availability. However, homogenous silver nanoparticle inks can lack the appropriate attributes required for robust printed physical sensors. In this work, we demonstrate that fully printed resistive temperature detector (RTD) sensors can benefit from ink hybridization. Specifically, we investigate RTDs printed by aerosol jet printing of hybrid nickel–copper-silver nanoparticle inks. We show that the overall sensitivity of the printed sensors can be enhanced through the introduction of these varied particles due to intentionally incorporated interfacial obstacles within the percolation network. While the temperature coefficient of resistance is decreased, the change in resistance per change in temperature can be maximized through the enhanced scattering provided by nickel and copper particle constituents. We report a sensitivity increase of 300% through utilizing 40% (by volume) mixture of silver and copper/nickel xylene-based inks. The results are corroborated through SEM/EDS analysis to understand the final weight percent of varied elements within the printed thin film. This magnitude of sensitivity opens up the possibility of utilizing printed RTDs for a wider range of sensing applications, where probing electronics are often low-cost.

Introduction

Printed electronics have been enhanced significantly by the progress of additive manufacturing (AM) techniques such as aerosol jet printing and inkjet printing.[1–4] Additionally, the formidable development in nanotechnology and nanomaterials has enabled new printable devices. Silver nanoparticle-based conductive inks have dominated the field of printed conductors due to their relatively low temperature processability, wide commercial availability, and good electrical conductivity after sintering.[5,6] There are some drawbacks to the use of Ag nanoparticle inks including susceptibility to corrosion in ambient environments,[7,8] electrochemical migration,[9] and the fact that the conductivity is sensitive to both strain and temperature.[10,11] Protective coatings may be used to passivate printed traces against humid environments. However, the fact that printed silver traces are sensitive to temperature can also be exploited for temperature sensing applications.[12]

It has been demonstrated that the temperature dependence of the carrier transport within conductive films can be capitalized on to form resistive temperature sensors, commonly known as resistive temperature detectors (RTDs) in the literature. The simplicity of the structure and the ease of characterization have resulted in this temperature sensing technique being widely used for many applications, specifically for high temperatures, where semiconducting-based sensors lack reliability. The most common method of fabricating these sensors is through photolithographic methods, as this allows one to have the high spatial resolution required to form geometries that allow for a measurable resistance. However, printing may be advantageous for RTDs, specifically in terms of cost, high throughput production, or substrate freedom.

Printed RTDs demonstrated in the literature have shown great promise for applications in human body temperature monitoring, wearable electronics, soft robotics, and large area thermal management of electric batteries and fuel cells.[13–16]

[a]Department of Electrical and Computer Engineering, University of Wisconsin-Madison, Madison, WI, 53706, USA. E-mail: joseph.andrews@wisc.edu
[b]Department of Mechanical Engineering, University of Wisconsin-Madison, Madison, WI, 53706, USA
†Electronic supplementary information (ESI) available. See DOI: https://doi.org/10.1039/d2nr04005k

Further, resistive temperature sensors printed on flexible substrates can be wrapped around curved surfaces to monitor the temperature of the curved objects more accurately. However, they have not been translated out of the lab due to their low sensitivity and baseline resistance, which ultimately precludes their integration with low-cost electronics.[17] One method of increasing the baseline resistance and overall sensitivity would be to utilize hybrid nanomaterial-based inks, which can effectively provide intentional interfacial defects that do not inhibit temperature sensitivity.

The idea of utilizing multiple nanomaterials within a printable ink has been explored for a number of applications recently. For example, researchers have utilized hybrid inks consisting of silver nanomaterials and high-aspect ratio materials such as carbon nanotubes to increase strain resilience.[18] Others have utilized silver nanoparticle–graphene hybrid ink to increase strain sensitivity, resulting in a high gauge-factor strain sensor.[19] These diametrically opposed applications demonstrate that through appropriate material selection, silver-nanoparticle hybrid inks can be designed and tuned to enhance a specific application.

While these hybrid inks, and others explored in the literature,[20,21] are unique in that they enable a new design method for printed electronics, the printability and robustness of the printed traces must be examined in more detail. So far, the focus of research in the field of hybrid conductive inks is to develop hybrid inks with high electrical conductivity at lower sintering temperature,[22] high optical transparency,[23] mechanical stretchability,[18] or resistance to oxidation.[24] To the best of our knowledge, no experimental results have been reported related to temperature dependent resistivity of the printed traces with metallic nanoparticle hybrid inks in the literature. Additionally, most of the fabrication techniques used in those experiments are not material efficient or scalable. Additive manufacturing techniques, such as aerosol jet printing (AJP) can facilitate the hybrid ink fabrication process due to its advantages including material efficiency, fast prototyping ability, compatibility with a wide range of solvents, and scalability.

To this end, we are interested in increasing the overall sensitivity (defined as the change in resistance per change in temperature) through the use of a hybridized silver nanoparticle ink while maintaining compatibility with the aerosol jet printing technique. To accomplish this, we utilize hybrid inks that contain other transition metal nanoparticles due to their compatibility with the solvent vehicle and printing method, allowing for high throughput processability. The specific transition metals that will be incorporated in the hybrid inks are nickel and copper.

Transitional metal nanomaterials such as nickel (Ni), and copper (Cu) nanoparticles are potential candidates due to their solution processability and high sintering temperature around of 900 °C.[25] The high sintering temperature ensures that they will not contribute to the conductive percolation network of a homogenous silver nanoparticle thin film, given that the sensor is not subjected to temperatures above 400 °C because

of substrate degradation.[26] Additionally, nickel nanoparticles have the added benefit of being corrosion resistant, which could lead to effective passivation within the thin film, reducing the impact of humidity.

In this paper, we demonstrate a facile way to develop hybrid conductive inks with a tunable temperature coefficient of resistance (TCR) and sensitivity for printed resistive temperature sensors by aerosol jet printing hybrid conductive inks composed of Ag, Cu, and Ni nanoparticles. First, we studied the morphological and elemental differences in printed thin films containing various volume fractions of two commercially available inks; one with silver nanoparticles only and one with a mixture of Ni and Cu nanoparticles. Next, we characterized the resistance dependence on temperature and used these tests to calculate the temperature coefficient of resistance and the overall sensitivity. Ultimately, our results showed that it is possible to tune the TCR value from 1.04×10^{-3} (°C^{-1}) to 2.35×10^{-3} (°C^{-1}) and the sensitivity of the printed temperature sensors from 0.15 (Ω °C^{-1}) to 0.59 (Ω °C^{-1}) solely by adjusting the composition the hybrid conductive ink.

Results and discussion

Aerosol jet printing resistive temperature sensors

All the sensors were printed using the aerosol jet printing technique as described in detail in the Experimental section. A schematic of aerosol jet printing along with the RTD pattern is shown in Fig. 1. In the print process, the hybrid ink is aerosolized by ultrasonic sonication, which excites the liquid ink into an aerosol of droplets on the order of 1–5 μm in diameter. Next, the ink is taken to the nozzle using an inert carrier gas, where it is subsequently focused using a secondary sheath gas. The droplet-laden convergent gas flow is accelerated at the nozzle tip, resulting in a high-speed flow that allows for transport to the substrate at a standoff distance of 4 mm. Line width, thickness, and overspray of the printed traces depend on print process parameters such as carrier gas flow rate, sheath gas flow rate, atomizer current, stage speed, and stage temperature. A detailed investigation of optimizing aerosol jet
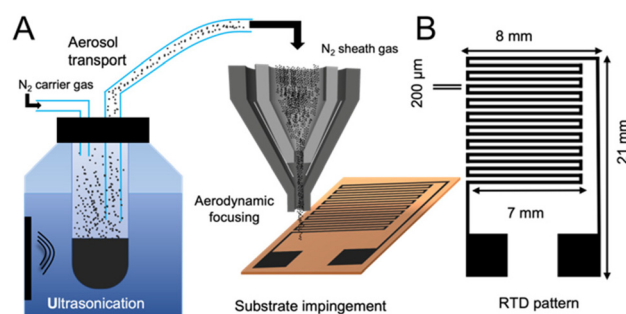

Fig. 1 Aerosol jet printing resistive temperature sensors. (A) Schematic depicting the steps of aerosol jet printing including the ultrasonication, transport, aerodynamic focusing and substrate impingement. (B) The geometry of the RTD sensors designed to be printed.

printed thin film traces was given in the work of Mahajan *et al.*[27] In this study, we fine-tuned the printing parameters such as carrier gas flow rate, sheath gas flow rate, and stage speed to ensure print quality, with each different ink requiring slightly different parameters to achieve the same line resolution, which was approximately 75 μm. Using this technique, serpentine traces were printed to maximize the total resistance per unit area while keeping the total sensor area minimum to allow for temperature sensitivity. A digital photograph, optical micrograph, and SEM image of a representative printed temperature sensor from the hybrid ink is shown in Fig. 2. From Fig. 2, it is clear that traces are well defined, and the overspray is minimal.

EDS analysis

One challenge with aerosol jet printing is selective aerosolization. For example, specific particles may have a higher probability of being up-taken within a droplet, based on their size and overall density. To investigate the elemental composition of the hybrid ink with different Ni–Cu ink volume percent, the hybrid ink was aerosol jet printed on Kapton film and baked at 260 °C for 1 hour, then Energy Dispersive Spectroscopy (EDS) analyses were performed, and the results are shown in Fig. 3. The Ag weight percent decreased and Ni, Cu weight percent increased with the increase of the Ni–Cu ink volume percent, which is as expected. Fig. 3 also confirms that the Ni–Cu ink has more Cu than Ni. The EDS element mapping data is given in the ESI.† From the elemental mapping results, we can see that the Ni, and Cu nanoparticles are uniformly distributed within the traces of the printed resistive temperature sensors, which ensures device to device performance stability of the printed sensors (Fig. S2†).

TGA analysis

Thermogravimetric analysis (TGA) can provide important insight into material decomposition by measuring the mass change over temperature.[28] Organic binders are widely used in conductive inks to modify ink viscosity and surface tension to improve printability. However, left-over organic binders after heat treatment of the printed traces can significantly degrade the electrical performance of the printed devices. In addition, the relatively small TCR of the printed resistive temperature
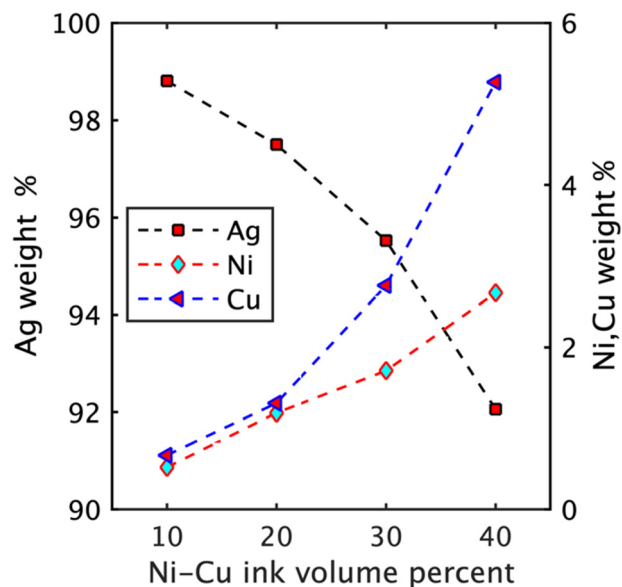

Fig. 3 Effect of volumetric ink modification on the weight% observed within printed thin films measured using EDS.

sensors printed with Ag nanoparticle ink compared to that of the bulk Ag accounted for the left-over organic binders after heat treatment. To evaluate the amount of left-over organic binders, TGA measurements were carried out for sensors printed with inks that had varied compositions. The detail of the TGA analysis was given in the methods section and the results were given in Fig. S3,† which indicates that there is no significant mass change in the temperature range from 200 °C to 400 °C. The decomposition temperature of the commonly used binders is also in the range of 200 °C to 400 °C. Thus, the heat treatment method employed in this study is effective to remove the left-over organic binders. It is clear from Fig. S3† that the Kapton substrate did not decompose until the temperature reached 500 °C, which confirms that the Kapton substrate is a good choice for high temperature applications.

Temperature characterization

To investigate the TCR of the conductive traces printed with the hybrid conductive ink, resistive temperature sensors were
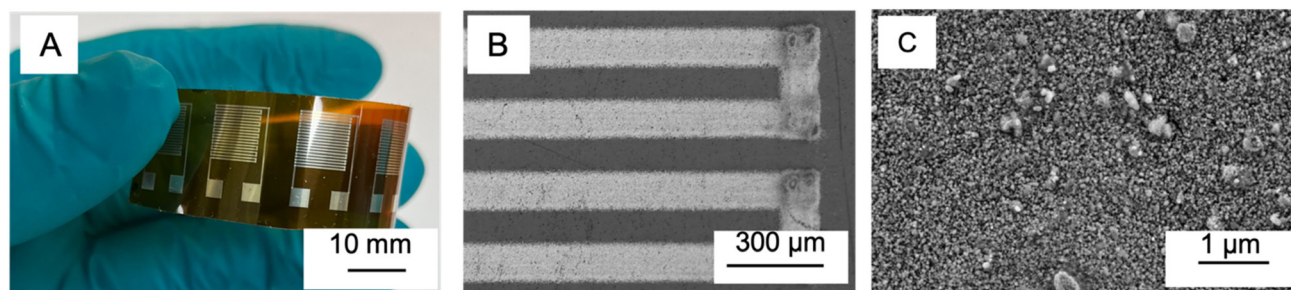

Fig. 2 Aerosol jet printed resistive temperature sensor utilizing hybrid transition metal inks. (A) Digital image of an array of temperature sensors printed on a flexible substrate. (B) Optical micrograph, and (C) SEM image of the hybridized thin film printed with 10% ink.

aerosol jet printed onto Kapton substrates in a meander line shape with dimensions shown in Fig. 1. The total trace length is 156 mm, the trace width is 200 μm and the total sensor area is 168 mm² including connection pads. Optical profilometry measurements suggest that the trace thickness is approximately 0.40 μm (Fig. S1C†). The details of profilometry measurements are given in ESI.† After printing, the sensors were baked at 260 °C for 1 hour. This allows for the sintering of the silver nanoparticles but does not facilitate the sintering of either the copper or nickel nanoparticles, ensuring that they will act as defects within the thin film. Rahman *et al.*, used X-ray photoelectron spectroscopy (XPS) to investigate the oxidation of aerosol jet printed Ag nanoparticles during annealing at up to 500 °C in ambient atmosphere and concluded that Ag nanoparticles annealed at such high temperature did not oxidize.[29] Next, resistance temperature measurements over time were performed for the heating and cooling cycles as described in the Experimental section and the results were shown in Fig. 4. The rate of heating was uncontrolled, but on average it took 1.5 hours for the heating process and 6 hours for the cooling process. The long cooling time stems from the passive nature of the cooling procedure. Due to the slow heating/cooling, the transient response of the sensor can be ignored.

From Fig. 4, we can see that resistance for all sensors varies linearly with temperature (from 22 °C to 150 °C) for heating and cooling cycles. The primary differences between the sensors' responses are the baseline resistance and the slope of the linear correlation between resistance and temperature. The baseline resistance increases with the added Ni/Cu content, and the overall slope increases as well. This is evidence of the Ni/Cu nanoparticles serving as defect sites that disrupt the percolation transport. The slope, or resistance change calculated as is $\Delta R = R - R_n$, where R_n is the resistance of the sensor at room temperature and R is the resistance of the sensor at 150 °C, for each sensor is plotted in Fig. 4F. ΔR is ultimately a function of both the temperature coefficient of resistance and the baseline resistance. This relationship is explored in the subsequent section.

Hysteresis for the sensors is observed as seen in Fig. 4(A, B, and D). This is expected, as these sensors are not passivated, and the silver nanoparticles are sensitive to the ambient environment. Interestingly, the hysteresis is significantly reduced for the sensors with both 20% and 40% Ni Cu content. This could be an effect where the more inert nanoparticles are serving as an in-film passivation element. However, this effect is not explored in detail, and it is expected
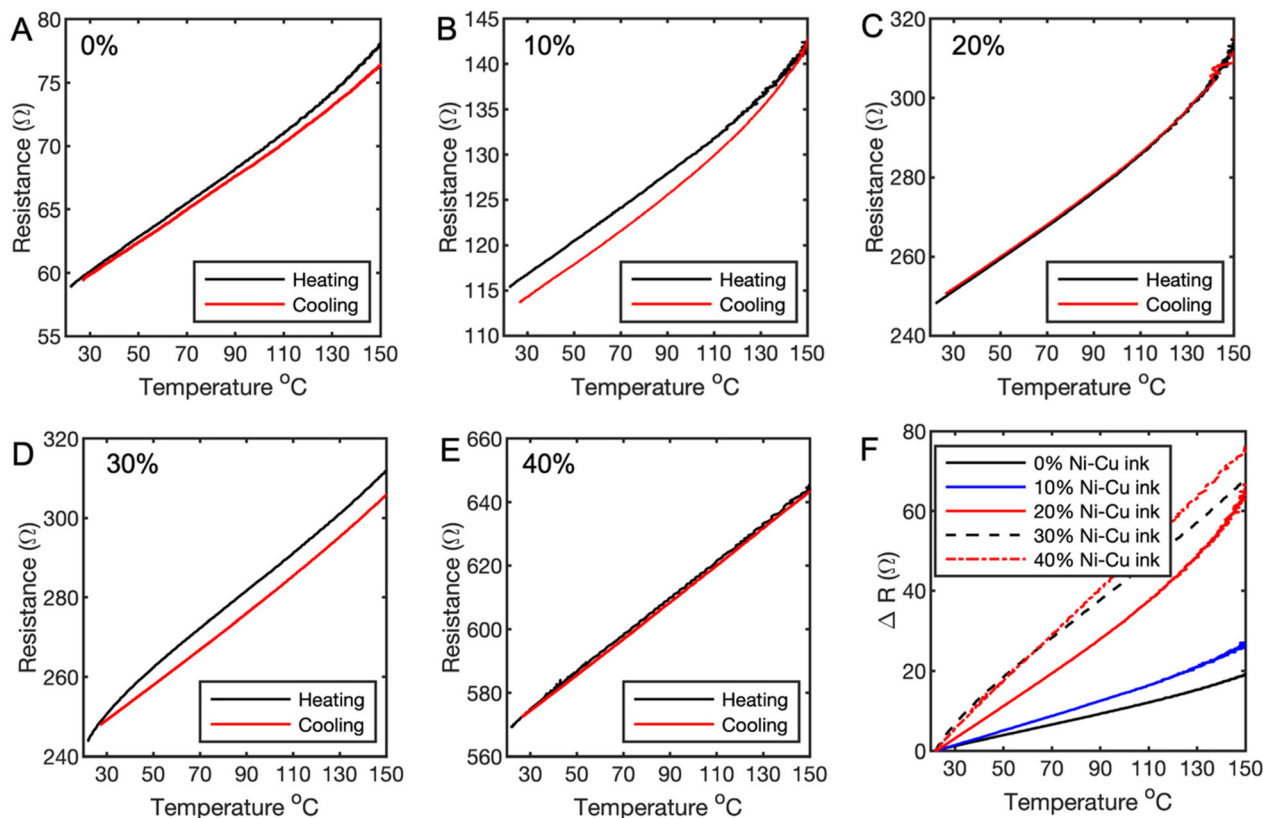

Fig. 4 Resistance-temperature measurement results for resistive temperature sensors aerosol jet printed with various inks both for heating and cooling cycles. Various hybrid inks with added Ni−Cu ink volumetric percentages ranging from 0% to 40% are measured and displayed as follows: (A) 0% Ni−Cu ink (B) 10% Ni−Cu ink, (C), 20% Ni−Cu ink, (D) 30% Ni−Cu ink, (E) 40% Ni−Cu ink. (F) Comparison of resistance change with respect to temperature for various inks.

that for application the sensors would require a passivation scheme.

Temperature dependent electrical resistivity of printed NP films

Temperature dependent electrical resistivity of metals is well known.[30,31] Generally, the resistance of metals increases with temperature which is known as positive temperature coefficient behavior. However, the temperature dependency of bulk metals depends on their crystal structure and grain size. For example, Qin *et al.*, showed that temperature dependence of resistance of nanostructured Ag depends on grain size and density.[32] In the case of metallic thin films, the thickness of the metal films affects its temperature coefficient of resistance due to the surface scattering of electrons, which is a known size effect.[33–35] For printed metallic nanomaterial films, film density, residual organic binders, and film morphology plays an important role both for film resistance and temperature coefficient of resistance.

TCR and sensitivity are the two important figure-of-merit for resistive temperature sensors. TCR is defined in eqn (1) as:

$$TCR = \frac{(R - R_0)}{R_0(T - T_0)} \tag{1}$$

where R is the resistance at the temperature T and R_n is the resistance at T_n TCR is dependent on the atomic structure of the metal nanoparticles in the ink as well as the printed thin film properties such as film density, thickness, and width. For thin metallic film conductors, according to Matthiessen's rule, the film resistance is given in eqn (2) as

$$R_{\text{total}} = R_{\text{defect}} + R_{\text{phonon}} \tag{2}$$

where R_{defect} is the resistance due to the carrier scattering by impurities in conductive film and R_{phonon} is the resistance due to phonon scattering.[36] The Cu and Ni nanoparticles in the film act as defect points which ultimately induce carrier scattering. This scattering results in the increase of the resistance of the film at room temperature. As the volume percent of the Ni–Cu ink increases, the defect density also increases, leading to much higher initial resistance values. Also, R_{defect} dominates R_{phonon} as the volume percent of the Cu–Ni ink increases in the hybrid ink and the TCR decreases.

Interestingly, the TCR of the thin film does not decrease at the same rate that the baseline resistance increases. This fact implies that through the introduction of nanoparticle defects the resistance due to phonon scattering is also increased. This likely stems from an effect where the introduction of the nanoparticles modifies the percolation pathway of the constituent nanoparticle thin film, increasing the phonon scattering at the silver NP to silver NP junctions. Ultimately, the fact that the baseline resistance increases at a faster rate than the TCR decreases allows the sensitivity of the printed RTDs to be increased.

In this work, the sensitivity is defined practically as the change in resistance with respect to change in temperature, shown in eqn (3).

$$Sensitivity = \frac{(R - R_0)}{(T - T_0)} \tag{3}$$

We can also relate this sensitivity to the TCR of the thin film and the baseline resistance as shown in eqn (4).

$$Sensitivity = TCR \times R_0 \tag{4}$$

Here we can directly see that by increasing R_0 at a faster rate than the TCR decreases we can maximize and control sensi-
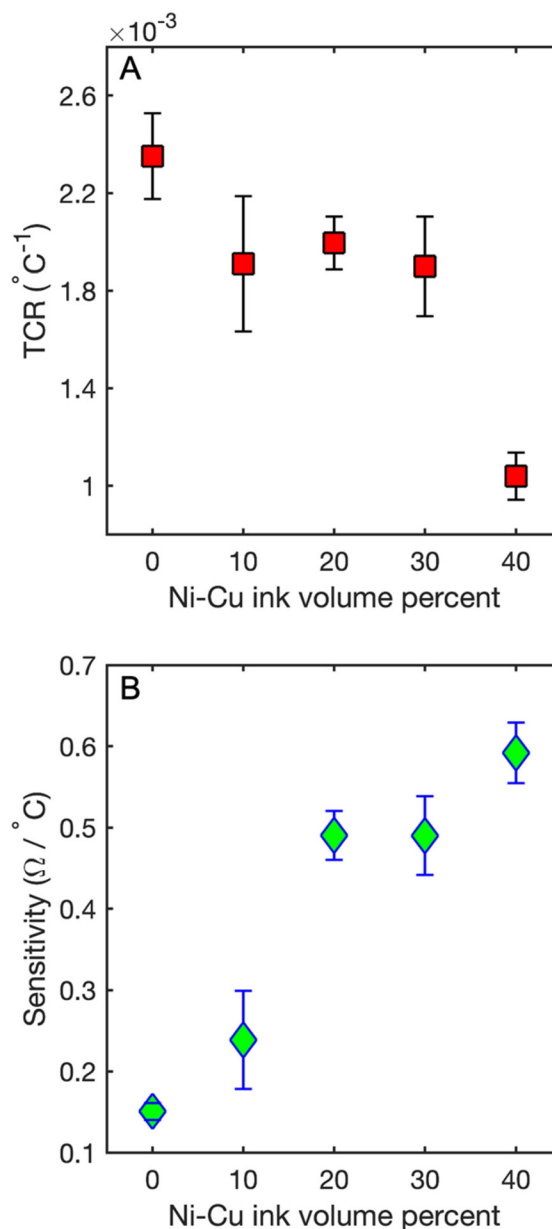

Fig. 5   TCR (A) and sensitivity (B) of aerosol jet printed resistive temperature sensors *vs.* ink composition.

tivity. The TCR and sensitivity for all sensors with different ink compositions are calculated from at least 5 different temperature tests for each sample and the mean average and the standard deviation of the results are plotted in Fig. 5. From Fig. 5, we can draw the following conclusions: (1) TCR is maximum for the sensors printed with silver nanoparticle ink and the max TCR = $2.35 \times 10^{-3} \pm 1.76 \times 10^{-4}$ (°C^{-1}). (2) TCR decreases with the increase of Ni–Cu ink volume in the hybrid ink. (3) Sensors printed with silver nanoparticle ink have the minimum sensitivity of 0.15 ± 0.01 (Ω °C^{-1}) and the sensitivity increased to 0.59 ± 0.03 (Ω °C^{-1}) for the sensors printed with the hybrid ink with 40% Ni–Cu nanoparticle ink. It is noticed that the TCR of the sensors printed with silver nanoparticle ink is greater than those reported in the literature.[37] This is likely due to the higher sintering temperature and longer sintering time. Also, the TCR of the printed resistive sensors strongly depends on the ink composition as we demonstrated within this work. The comparison of the reported TCR and sensitivity in this work with respect to published data in the literature is given in Table S1.† Only data from aerosol jet or inkjet printed resistive temperature sensors with Ag nanoparticle ink is included in Table S1† to ensure comparability. While we do not have the highest TCR or sensitivity, we present a facile method for directly tuning the response using hybrid inks.

The more practical defined sensitivity is an important parameter from an engineering application perspective, and ultimately, having a high TCR does not necessarily imply a high practical sensitivity. For printed electronics to be viable as lower-cost alternatives to lithographically produced sensors, the interrogation electronics must also be low-cost. Therefore, maximizing the change in resistance effectively makes the sensors easier to measure when using lower-cost analog-to-digital converters. A common method for interrogating resistance-based temperature sensors is to utilize a constant current and measure the resulting voltage. The resistance is calculated using Ohm's law and the temperature is inferred. By maximizing the change in resistance one can effectively maximize the change in voltage, ensuring the signal is affected less by voltage bias and drift, a common occurrence in lower-cost interrogation electronics.

Printed temperature sensor performance in humid environment

Stable operation of printed sensors in various environmental conditions is crucial for their adoption in engineering design processes. Relative humidity (RH) is one of the common variable environmental parameters. To evaluate the stability of the aerosol jet printed temperature sensors in humid environment and the effect of passivation, sensors printed with 0% and 20% Ni–Cu hybrid ink were spin coated with a 5 μm thick layer of Polyimide. Both the sensors with and without passivation were temperature cycled in the temperature range from room temperature to 85 °C under RH = 75% and the result were given in Fig. 6(A). From Fig. 6(A) we can see that resistance of the both passivated and non-passivated sensors change linearly with the temperature for both sensors printed with 0% and 20% Ni–Cu ink and the effect of passivation is
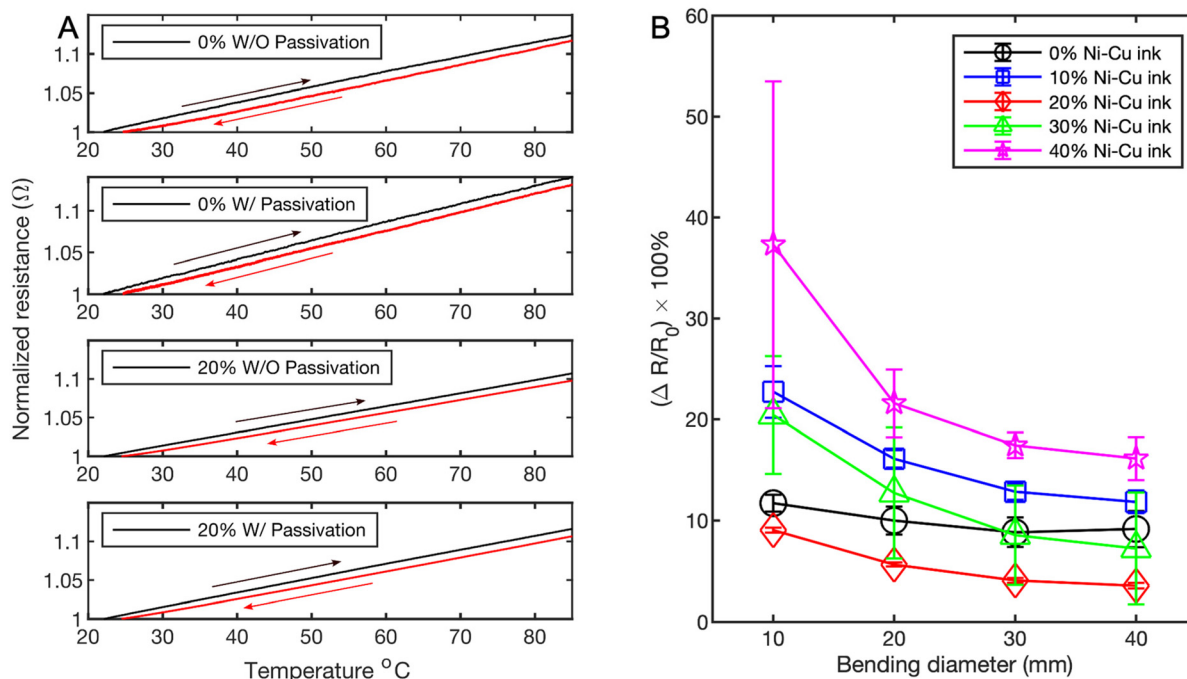

Fig. 6 Effect of passivation and bending strain on aerosol jet printed temperature sensors with hybrid inks. (A) Temperature cycling test for sensors printed with 0% and 20% Ni–Cu ink with and without Polyimide passivation, RH = 75%. (B) Normalized resistance change percentage with respect to different bending diameter for sensors printed with different hybrid inks.

Table 1 Hybrid ink composition

Ink	Ag NP ink (mL)	Ni–Cu NP ink (mL)	Terpineol (mL)
Ink 1	2	0	0.2
Ink 2	1.8	0.2	0.2
Ink 3	1.6	0.4	0.2
Ink 4	1.4	0.6	0.2
Ink 5	1.2	0.8	0.2

not very significant. However, the passivation can provide a protective layer for the printed sensors against mechanical scratches. The sensor stability at harsh environments needs to be investigated further.

Printed temperature sensor response to bending strain

Printed resistive temperature sensors are also sensitive to mechanical strain. To characterize the response of the printed sensors with respect to bending strain, bending tests were performed as described in the methods section and the results are given in Fig. 6(B). Results from Fig. 6(B) show that normalized resistance change is different for sensors printed with different hybrid inks. The normalized resistance changes for the sensors printed with 20% Ni–Cu hybrid ink is minimum and that of the 40% Ni–Cu hybrid ink is maximum over different bending diameters. We hypothesize that two competing phenomena are affecting the response of the sensors to the bending strain. With the increase of the volume percent of the Ni–Cu ink, the printability of the hybrid ink degraded, and the printed films are susceptible to cracks if the film is subjected to mechanical strain. However, if the volume percent of the Ni–Cu ink increases to a certain threshold, then the Ni–Cu nanoparticles in the film printed with hybrid ink act as an interparticle strain relief site, which explains why the sensors printed with 20% hybrid ink showed the minimum normalized resistance change with respect to bending strain. If the volume percent of the Ni–Cu ink increases further, then the printability of the hybrid ink degrades even more and the percolation network between neighboring Ag nanoparticles will be more susceptible to bending strain, which explains the sensors printed with 40% hybrid ink have the maximum normalized resistance change over bending diameter.

Conclusion

In this paper, aerosol jet printing was used as a facile fabrication technique to pattern hybrid conductive inks for printed resistive temperature sensors. First, through EDS analysis we were able to correlate the thin-film weight percentage of a hybrid ink consisting of commercially available metallic nanoparticle inks. This analysis provides insight into the mixing and aerosol jet printing's effectiveness at depositing uniform distributions of hybrid inks. Next, we analyzed the temperature response of the hybrid thin films. Specifically, we demonstrated that through defect sites introduced by

varied metallic nanoparticles we can alter the thin film TCR and baseline resistance. The baseline resistance is modified more severely, which culminates in an enhancement of sensitivity. This is most evident in the RTD made from a 40% volume addition of the Ni–Cu ink, where the sensitivity is increased from approximately 0.15 Ohm °C^{-1} to 0.59 Ohm °C^{-1}. This sensitivity increase is important and ultimately required to translate printed RTDs to lower-cost settings where the interrogation electronics must also be low-cost.

Experimental

Materials

The silver nanoparticle ink used in this study was UTDAg25TE and it was purchased from UT Dots Incorporated. This formulation consists of silver nanoparticles dispersed in xylene with proprietary additives and adhesion promoters. The weight% of the Ag NPs is 45%. The Ni–Cu nanoparticle ink was Ni-UA70T and it was purchased from Nanomagic Incorporated. Their formulation is also in xylene and the particle loading of this ink is 25%, Kapton film is purchased from McMaster-Carr with a thickness of approximately 125 μm. Terpineol is purchased from Sigma Aldrich.

Ink preparation

Silver nanoparticle ink and Ni–Cu nanoparticle ink were mixed in a vial with different volume percent as shown in Table 1. 0.2 mL of Terpineol was added to adjust ink viscosity. The mixed inks were ultrasonicated for 1 hour using a Branson bath sonicator to ensure proper mixing of the hybrid inks. Then 2 ml of hybrid ink is transferred to the ink vial of the aerosol jet printer.

Aerosol jet printing

Resistive temperature sensor patterns were designed with commercial computer aided design software AutoCAD (Autodesk Inc.) and the patterns were further processed with VM tools, which is an AutoCAD add-on provided with the aerosol jet printer. Aerosol jet printing of AgNP/Ni–Cu hybrid ink was carried out using an Optomec AJ200 aerosol jet printer with an ultrasonic atomizer and a 200 μm nozzle was used for all the printings for this work. The sheath flow rate, and carrier gas flow rate were slightly adjusted for each ink composition and kept between 25–40 SCCM and 18–25 SCCM, respectively. The atomizer current was set to 0.5 Amps and the platen temperature was set to 60 °C, with a printing speed of 6 mm s^{-1}. Before printing, the Kapton substrate was cleaned with de-ionized water and IPA to remove dust and contaminants. One pass of AgNP/Ni–Cu NP hybrid ink was printed in a meandered shape to be used as a resistive temperature sensor. After printing, samples were baked at 260 °C degrees for 1 hour at ambient atmosphere to remove solvents and binders to make the traces conductive.

Temperature test

Temperature tests were performed inside a Thermo Scientific Lindberg/Blue M vacuum oven, where the printed temperature sensors were put alongside a commercial thermistor (Model number: 55004, Omega Engineering, Inc). The temperature testing was carried out in ambient atmosphere. The resistance of the printed temperature sensor and thermistor was measured with a Keysight source measurement unit (Keysight B2902, Keysight Inc.) over time. The printed resistive sensors were provided with 150 μA constant current and the thermistor was provided with 15 μA constant current to reduce self-heating related measurement errors. Data was collected by Keysight Easyexpert software. The temperature was calculated from the thermistor resistance using thermistor parameters provided by the vendor using the Steinhart-Hart equation.

SEM and EDS analysis

Aerosol jet printed samples were coated with 10 nm carbon using Leica ACE 600 deposition system (Leica Microsystems Inc.) to avoid charging effects during SEM imaging. SEM imaging is done with Zeiss LEO 1530 scanning electron microscope and EDS analysis were done with Ultradry EDS detector (Thermofisher Scientific Inc.). EDS data analysis was performed with Pathfinder X-ray microanalysis software from Thermofisher Scientific Inc.

TGA measurement

Around 10 mg of samples for each sensor printed with different ink is collected by cutting the heat-treated sensors into small pieces. Thermogravimetric analysis was carried out with TGA TA Q500 (TA instruments Inc.) using the Platinum pan under Nitrogen gas flow with a flow rate of 50 mL min^{-1}. The sample was heated from room temperature to 700 °C and the temperature ramp was at 20 °C min^{-1}. TGA data analysis was performed with TA instrument analyzer software and the exported data was plotted with MATLAB from MathWorks Inc.

Bending test

Printed sensors were fixed on cylindrical iron bars with diameters ranging from 10 mm to 40 mm and resistance was measured with a Fluke digital multimeter at room temperature. Three sensors for each ink composition were measured. A picture of the bending test measurement setup was given in Fig. S4.†

Humidity test

Humidity tests were carried out for sensors printed with 0% and 20% Ni–Cu hybrid ink. The sensors were divided into two subgroups. For group one, sensors were passivated by spin coating around 5 μm thick Polyimide and the second group was not passivated. The detail of polyimide passivation is given in ESI.† The humidity of the oven was controlled by saturated NaCl solution, which provides around 75% of relative humidity for a wide temperature range. The temperature cycling test was carried out as described in the temperature test section. During the humidity test, the maximum temperature was limited to 85 °C.

Author contributions

M. T. planned and carried out experiments, analyzed data, and prepared the manuscript. V. A. assisted in the fabrication and testing of the temperature sensors and reviewed the manuscript. A. M. assisted in the experimental analysis of the temperature sensors and reviewed the manuscript. J. A. assisted in the design of the experiments, the data analysis, and the preparation of the manuscript. All authors read the manuscript.

Conflicts of interest

There are no conflicts to declare.

Acknowledgements

References

1 Y.-T. Kwon, Y.-S. Kim, S. Kwon, M. Mahmood, H.-R. Lim, S.-W. Park, S.-O. Kang, J. J. Choi, R. Herbert, Y. C. Jang, Y.-H. Choa and W.-H. Yeo, *Nat. Commun.*, 2020, **11**, 3450.

2 T. Nga Ng, D. E. Schwartz, L. L. Lavery, G. L. Whiting, B. Russo, B. Krusor, J. Veres, P. Bröms, L. Herlogsson, N. Alam, O. Hagel, J. Nilsson and C. Karlsson, *Sci. Rep.*, 2012, **2**, 585.

3 W. Su, B. S. Cook, Y. Fang and M. M. Tentzeris, *Sci. Rep.*, 2016, **6**, 35111.

4 A. Ahmed Simon, B. Badamchi, H. Subbaraman, Y. Sakaguchi, L. Jones, H. Kunold, I. J. van Rooyen and M. Mitkova, *Sci. Rep.*, 2021, **11**, 1–15.

5 I. J. Fernandes, A. F. Aroche, A. Schuck, P. Lamberty, C. R. Peter, W. Hasenkamp and T. L. A. C. Rocha, *Sci. Rep.*, 2020, **10**, 8878.

6 K. Skarżyński, J. Krzemiński, M. Jakubowska and M. Słoma, *Sci. Rep.*, **11**, 18141.

7 V. J. Keast, *Appl. Nanosci.*, 2022, **12**, 1859–1868.

8 J. L. Elechiguerra, L. Larios-Lopez, C. Liu, D. Garcia-Gutierrez, A. Camacho-Bragado and M. J. Yacaman, *Metrologia*, 2018, **55**, L5–L11.

9 C.-H. Tsou, K.-N. Liu, H.-T. Lin and F.-Y. Ouyang, *J. Electron. Mater.*, 2016, **45**(12), DOI: **10.1007/s11664-016-5000-9**.

10 S. Zhang, L. Cai, W. Li, J. Miao, T. Wang, J. Yeom, N. Sepúlveda and C. Wang, *Adv. Electron. Mater.*, 2017, **3**, 1700067.

11 M. D. Dankoco, G. Y. Tesfay, E. Benevent and M. Bendahan, *Mater Sci Eng B Solid State Mater Adv Technol.*, 2016, **205**, 1–5.

12 L. Kang, Y. Shi, J. Zhang, C. Huang, N. Zhang, Y. He, W. Li, C. Wang, X. Wu and X. Zhou, *Microelectron. Eng.*, 2019, **216**, 111052.

13 J. K. Sim, J. Hyun, I. Doh, B. Ahn and Y. T. Kim, *Metrologia*, 2017, **55**, L5.

14 B. Li, M. H. Parekh, R. A. Adams, T. E. Adams, C. T. Love, V. G. Pol and V. Tomar, *Sci. Rep.*, 2019, **9**, 13255.

15 A. V. Quintero, F. Molina-Lopez, E. C. P. Smits, E. Danesh, J. van den Brand, K. Persaud, A. Oprea, N. Barsan, U. Weimar, N. F. de Rooij and D. Briand, *Flex. Print. Electron.*, 2016, **1**, 025003.

16 E. A. Ozek, S. Tanyeli and M. K. Yapici, *IEEE Sens. J.*, 2021, **21**, 26382–26388.

17 S.-Y. Kim, J.-D. Kim, Y.-S. Kim, H.-J. Song and C.-Y. Park, *Int. J. Control. Autom.*, 2015, **8**, 67–74.

18 K.-Y. Chun, J. Oh, J. Rho, J.-H. Ahn, Y.-J. Kim, H. R. Choi and S. Baik, *Nat. Nanotechnol.*, 2010, **5**, 853–857.

19 Y. Z. N. Htwe, I. N. Hidayah and M. Mariatti, *J. Mater. Sci.: Mater. Electron.*, 2020, **31**, 15361–15371.

20 N. Karim, S. Afroj, K. S. Novoselov and S. G. Yeates, *Sci. Rep.*, 2019, **9**, 8035.

21 C. Yim, Z. A. Kockerbeck, S. B. Jo and S. S. Park, *ACS Appl. Mater. Interfaces*, 2017, **9**(42), 37160–37165.

22 W. Yang, C. Wang and V. Arrighi, *J. Mater. Sci.: Mater. Electron.*, 2019, **30**, 11607–11618.

23 X. Chen, X. Wu, S. Shao, J. Zhuang, L. Xie, S. Nie, W. Su, Z. Chen and Z. Cui, *Sci. Rep.*, 2017, **7**, 13239.

24 D. Tomotoshi, R. Oogami and H. Kawasaki, *ACS Appl. Mater. Interfaces*, 2021, **13**(17), 20906–20915.

25 J. Hlina, J. Reboun and A. Hamacek, *Materials*, 2021, **14**(22), 7039.

26 DuPont Inc.

27 A. Mahajan, C. D. Frisbie and L. F. Francis, *ACS Appl. Mater. Interfaces*, 2013, **5**(11), 4856–4864.

28 N. Saadatkhah, A. C. Garcia, S. Ackermann, P. Leclerc, M. Latifi, S. Samih, G. S. Patience and J. Chaouki, *Can. J. Chem. Eng.*, 2020, **98**, 34–43.

29 M. T. Rahman, J. McCloy, C. v. Ramana and R. Panat, *J. Appl. Phys.*, 2016, **120**, 075305.

30 R. A. Matula, *J. Phys. Chem. Ref. Data*, 1979, **8**, 1147–1298.

31 E. H. Sondheimer, *Adv. Phys.*, 1952, **1**, 1–42.

32 X. Y. Qin, L. D. Zhang, G. S. Cheng, X. J. Liu and D. Jin, *J. Phys. D: Appl. Phys.*, 1998, **31**, 24–31.

33 W. Ma, *J. Phys. D: Appl. Phys.*, 2010, **43**, 465301.

34 F. Warkusz, *J. Phys. D: Appl. Phys.*, 1978, **11**, 2035.

35 K. Fuchs and H. H. Wills, *Math. Proc. Cambridge Philos. Soc.*, 1938, **34**(1), 100–108.

36 W. Steinhögl, G. Schindler, G. Steinlesberger, M. Traving and M. Engelhardt, *J. Appl. Phys.*, 2005, **97**, 023706.

37 M. Alhendi, R. S. Sivasubramony, D. L. Weerawarne, J. Iannotti, P. Borgesen and M. D. Poliks, *Adv. Eng. Mater.*, 2020, **22**, 2000520.